REPORT DOCUMENTATION PAGE

Form Approved OMB NO. 0704-0188

1. REPORT DATE (DD-MM-YYYY)	2. REPORT TYPE	3. DATES COVERED (From - To)
29-10-2018	Final Report	1-Oct-2013 - 30-Mar-2017

4. TITLE AND SUBTITLE
Final Report: Materials design. Optical interactions in virus-based materials

5a. CONTRACT NUMBER
W911NF-13-1-0490

5b. GRANT NUMBER

5c. PROGRAM ELEMENT NUMBER
611102

6. AUTHORS

5d. PROJECT NUMBER

5e. TASK NUMBER

5f. WORK UNIT NUMBER

7. PERFORMING ORGANIZATION NAMES AND ADDRESSES
Indiana University at Bloomington
509 East 3rd ST

Bloomington, IN 47401 -3654

8. PERFORMING ORGANIZATION REPORT NUMBER

9. SPONSORING/MONITORING AGENCY NAME(S) AND ADDRESS (ES)
U.S. Army Research Office
P.O. Box 12211
Research Triangle Park, NC 27709-2211

10. SPONSOR/MONITOR'S ACRONYM(S)
ARO

11. SPONSOR/MONITOR'S REPORT NUMBER(S)
62436-MS.8

12. DISTRIBUTION AVAILIBILITY STATEMENT
Approved for public release; distribution is unlimited.

13. SUPPLEMENTARY NOTES
The views, opinions and/or findings contained in this report are those of the author(s) and should not contrued as an official Department of the Army position, policy or decision, unless so designated by other documentation.

14. ABSTRACT

15. SUBJECT TERMS

16. SECURITY CLASSIFICATION OF:			17. LIMITATION OF ABSTRACT	15. NUMBER OF PAGES	19a. NAME OF RESPONSIBLE PERSON
a. REPORT	b. ABSTRACT	c. THIS PAGE			Bogdan Dragnea
UU	UU	UU	UU		19b. TELEPHONE NUMBER 812-856-0087

RPPR Final Report
as of 31-Oct-2018

Agency Code:

Proposal Number: 62436MS **Agreement Number: W911NF-13-1-0490**
INVESTIGATOR(S):

Name: Ph.D Bogdan Dragnea
Email: dragnea@indiana.edu
Phone Number: 8128560087
Principal: Y

Organization: **Indiana University at Bloomington**
Address: 509 East 3rd ST, Bloomington, IN 474013654
Country: USA
DUNS Number: 006046700 EIN: 356001673
Report Date: 30-Jun-2017 Date Received: 29-Oct-2018
Final Report for Period Beginning 01-Oct-2013 and Ending 30-Mar-2017
Title: Materials design. Optical interactions in virus-based materials
Begin Performance Period: 01-Oct-2013 **End Performance Period:** 30-Mar-2017
Report Term: 0-Other
Submitted By: Ph.D Bogdan Dragnea Email: dragnea@indiana.edu
Phone: (812) 856-0087

STEM Degrees: **STEM Participants:**

Major Goals: The major goals of the project were to:

1) Construct a photothermal microscope for manipulating nanoparticles through optical forces and measure their optical scattering and absorption spectra as they organize under optical radiation forces.

2) Engineer a coherent array of hundreds of light emitting molecules supported by a symmetric biomolecular template formed of a virus capsid.

3) Determine conditions required for collective relaxation and the nature of light emitted (coherence, dynamics), i.e. conditions in which the fluorophores act as an optical antenna array. Identify photonic and molecular structure characteristics, specifically the role of symmetry leading to super-radiance.

4) Assemble the super-radiant virus-like particle around a plasmonic nanoparticle and determine how the chromophore array couple to radiation and localized plasmon modes.

5) Measure collective absorption cross-section using the instrument developed in aim (1), and the samples of aim (2) and (4). Develop collective coupling model based on findings.

Accomplishments: We have published 6 papers related to different aspects of the 4 broader goals. We have a patent related to an application that is emerging from goals 3-4. Highlights from unpublished work are:
- discovery of collective relaxation at room temperature from a virus-supported fluorophore array. Radiation appears to be temporally coherent. A manuscript is under consideration at Nature.
- proof-of-principle for detection of nanoparticle-induced phase transformation in molecular materials using photothermal. The new approach should be of interest for technologies related to nanoparticle-sensitized bolometers. Manuscript in final form.

RPPR Final Report
as of 31-Oct-2018

Training Opportunities: Trainees:
- Joseph Holmes, Ph. D. candidate, 3rd year, Physics, IU. Has been enrolled in the APS Bridge program for underrepresented groups.
- Maryam Zahedian, Ph. D. candidate, 5th year, Chemical Physics, IU.
-Sajnee Desai, undergraduate, pursuing double major Chemistry and Physics, Honors.
- Sidra Ahmad, undergraduate, pursuing double major Chemistry and Physics, Honors. Nominated for the Goldwater scholarship.
- Amberly Xie, freshman, IU STARS program.

We have created two demos which have been used at the Wonderlab Science museum and at the Bloomington Science Fest, October 2018.

Results Dissemination: Invited talks (2015-2018):
- SPIE San Diego, August 2018
- International Center for Theoretical Physics (ICTP) Trieste, June 2017.
- Lehigh University, Chemistry Department invited talk, October 2018.
- Ohio University, Athens, Chemistry Department invited talk, May 2018.
- International Center for Theoretical Physics, Trieste, 2017
- Eindhoven Technical University, Netherlands, 2017
- University of North Carolina, Charlotte, 2016
- Harvard University, SEAS, 2015
- DOE Contractor meeting, Boston, 2015
- Aspen Center for Physics, 2015
- Berea College, 2015

Honors and Awards: IU Trustees Teaching Award

Protocol Activity Status:

Technology Transfer: Patent application, August 2018

title: Virus-enabled targeted vector for imaging, August 2018

PARTICIPANTS:

Participant Type: Postdoctoral (scholar, fellow or other postdoctoral position)
Participant: Irina Tsvetkova
Person Months Worked: 1.00 **Funding Support:**
Project Contribution:
International Collaboration:
International Travel:
National Academy Member: N
Other Collaborators:

DISSERTATIONS:

RPPR Final Report
as of 31-Oct-2018

Publication Type: Thesis or Dissertation
Institution: Indiana University
Date Received: 31-Oct-2016 Completion Date: 10/28/16 2:01AM
Title: "STRUCTURE AND MECHANOCHEMISTRY OF" "ICOSAHEDRAL VIRUSES AND VIRUS SHELLS STUDIED" "BY ATOMIC FORCE MICROSCOPY"
Authors: Cheng Zeng
Acknowledged Federal Support: **Y**

Collective emission from arrays of virus-supported chromophores

Irina B. Tsvetkova[a], Arathi Anil Sushma[a], Joseph C.-Y. Wang[b], William L. Schaich[c], and Bogdan G. Dragnea[a]*

[a]Chemistry Department, Indiana University Bloomington, IN, 47405, USA

[b]Department of Molecular and Cellular Biochemistry, Indiana University Bloomington, IN, 47405, USA

[c]Physics Department, Indiana University Bloomington, IN, 47405, USA

*Correspondence and requests for materials should be addressed to B.D. (email: dragnea@indiana.edu)

Over the years, spectacular improvements in chromophore photostability, wavelength range, biological integration, detectors and detection techniques, have pushed the limits of fluorescence imaging to realms never thought possible before[1-3]. Despite these improvements, most fluorescence imaging techniques continue to rely on the incoherent spontaneous emission from many independent chromophores. However, a system's collective behavior can be much more than the sum of its parts[4]. For instance, the indistinguishability of microscopic quantum constituents can lead to coherent behavior via quantum, symmetry-enforced selection rules[5]. Such collective relaxation processes can be much faster and more efficient than those encountered near the thermodynamic limit. Indeed, certain molecular phenomena that are central to life on earth appear to rely on quantum coherence[6]. Thus, light-harvesting complexes - macromolecular assemblies in photosynthetic organisms, exploit the tight spatial organization of proteinaceous multi-chromophore assemblies to enable coherent exciton transport in short times and over distances many times larger than the size of molecular constituents[7,8]. In a similar yet distinct vein, here we show that harnessing of organizational

principles present in viruses leads to collective behavior, in the form of coherent optical emission from hundreds of chromophores bound to a nanoscopic molecular framework. Thus, while at first fluorescence quenching ensues as the number of chromophores chemically-conjugated to the surface of a virus particle increases, when the number of chromophores per particle is nearing the maximum number of surface sites allowable, a sudden brightening of the emitted light and a shortening of the excited state lifetime are observed. This radiation brightening is observed under short pulse excitation only; steady-state excitation is characterized by conventional concentration quenching for any number of chromophores per particle. The results are consistent with efficient, collective relaxation at room temperature when the emitters are placed on a symmetric template, suggesting a way towards novel, virus-enabled imaging vectors with qualitatively different optical properties than state-of-the-art agents. Such biophotonic particles could be of interest for laser-guided surgery[9,10], optogenetic manipulation[11], and other applications that would benefit from bright, deep-subwavelength light sources[12].

Control of the probability of spontaneous emission through cooperation among emitters has a venerable history, and includes phenomena such as stimulated emission and lasing, super-radiance, amplified spontaneous emission, photon echo, and magnetic resonance decay. Most of these phenomena have been already worked into powerful spectroscopy tools [13,14].

In super-radiance (SR)[15-17], a sub-wavelength ensemble of indistinguishable, excited two-level quantum emitters is prepared in, or spontaneously attains, a correlated state which couples into a common electromagnetic field as a single, massive radiating dipole[18]. Because of

its substantially-accelerated radiative decay as the number of cooperating chromophores increases, in the years before the invention of the laser, SR was suggested as a way towards generating short coherent pulses of light, without a cavity. However, this promise has proven difficult to fulfill. The reason is that the coherent behavior emerges only when the quantum emitters are indistinguishable and the cooperative radiative decay of the system is faster than any other phase breaking (decoherence) process. Thus, SR could be observed at low temperature only for non-interacting (non-aggregated) emitters such as atomic gases[16], molecular centers in crystals[19], and quantum dots[20]. On the other hand, tightly bound molecular crystals and arrays[21] and in the light-harvesting complexes of certain photosynthetic microorganisms[8] exhibit accelerated radiative decays from excitonic states at close to room temperature. Only recently, coherent relaxation at room temperature was observed in ensembles of non-interacting (sparse) diamond N-vacancies[22].

Here we present experiments suggesting that coherent relaxation of non-interacting emitters at room temperature can even occur in soft matter, namely in arrays of molecular dyes, provided two conditions are present: 1) Excitation is done by high-intensity pulsed irradiation, and 2) the dyes are located on, and interacting strongly with a three dimensional, symmetric molecular scaffold of a size much smaller than the wavelength of light. Condition (2) presumably ensures the equivalence of local environments and thus optical indistinguishability of individual chromophores, while condition (1) ensures that initially nearly all chromophores are in the excited state. We note that these experimental design features represent a molecular assembly embodiment of the so-called “Dicke optical bomb”[4].

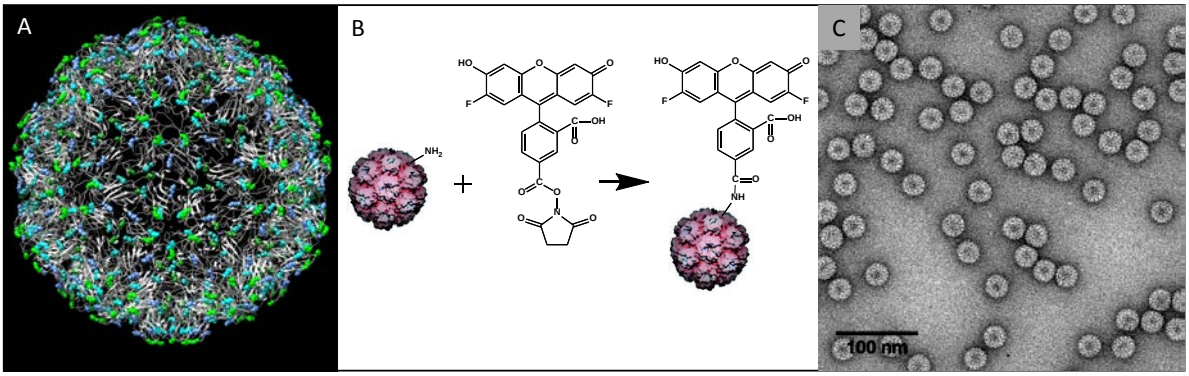

Figure 1. A) Molecular model of BMV with structure surface exposed lysines. B) Lysine bioconjugation reaction scheme. C) TEM image of near-saturation labeled BMV.

The symmetric molecular scaffold or template in this work is a Brome mosaic virus (BMV) particle, which has an icosahedral capsid formed of 180 identical self-assembled proteins[23]. A common bioconjugation reaction of surface-exposed lysines was used to covalently attach the fluorescein derivative dye, Oregon Green™ 488 carboxylic acid succinimidyl ester (OG), at specific locations on the virus (Fig. 1A, B, SI)[24]. The average number of chromophores was controlled by varying the molar ratio between capsid and dye in the reaction media, and by adjustment of buffer conditions (SI).

The degree of labeling was estimated from UV/Visible absorption spectra of purified BMV-chromophore conjugates (Fig. 2A) and confirmed by matrix assisted laser desorption/ionization-time of flight spectrometry (MALDI-TOF) (SI). From the molecular structure of the virus particle (Fig. 1A), based on steric constraints, we expect a maximum of N_{max}=300 chromophores per particle. The smallest distance between two nearest-neighbors at this labeling density is ~19 Å (see table in Fig. SI-1). Therefore, unlike the case of J and H molecular aggregates[25], negligible nearest neighbor electronic coupling is expected here. Indeed, no changes in the form of spectral shifts or broadening/narrowing of the bands could

be observed in the absorption and emission spectra as a function of *N,* at low excitation intensity (Fig. 2). Concentration quenching was, however, noticeable (see Fig. 2B, inset). This is consistent with previous works[23], although, as reported for other dye-labeled virus-like particles[26], the quenching rate was below that typically observed in free-dye solutions.

Absorbance spectra showed a bathochromic shift for the main absorbance peak of dye-conjugated BMV samples, independent of N, from 491 nm for the free dye to 496 nm, indicating that the dye is coupled to the protein (Fig. 2A). To obtain further information on the dye-surface geometry we attempted single particle reconstruction of cryo-electron microscopy images. The structures of BMV and dye-saturated BMV are indistinguishable at the 7 Å resolution of our experiment (Fig 1C, SI). Interestingly, although no extra density could be attributed to the presence of OG molecules, the OG-conjugated BMV particles (BMV-OG) are more stable to physical and chemical manipulations than wtBMV. Specifically, when dialyzed in disassembly buffer conditions for 24 hours, wtBMV is completely disassembled, while dye-saturated BMV remains intact, with no noticeable morphological changes (SI). The added

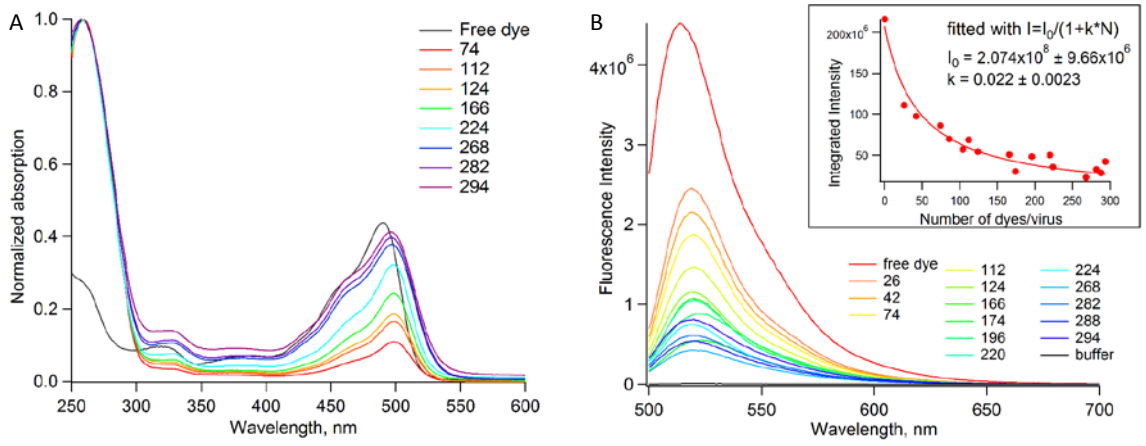

Figure 2. A) Uv-vis absorption and B) fluorescence emission spectra of free dye and BMV-OG. Inset in B) shows fit corresponding to the Stern-Volmer equation describing concentration quenching for spectrally-integrated, steady-state fluorescence intensity vs N.

resilience of the BMV-OG particles to environmental challenges suggests that the chromophores interact strongly with the capsid, in a way that stabilizes it.

Since the emission rate of an ensemble of coherent radiators is a nonlinear function of the number of excited chromophores and because the dephasing rate scales as *N*, coherent behavior will be favored under strong population inversion and/or reduction of dephasing rates. To obtain a strong population inversion, we have used pulsed excitation from a supercontinuum laser (120 ps pulse duration, maximum 500 μW average power at the sample). To investigate the possible onset of accelerated emission, we measured an effective fluorescence lifetime as estimated from the mean photon arrival times, and the time-integrated photon counts from single BMV-OG particles as a function of the average *N*, by fluorescence lifetime microscopy (FLIM) with time-correlated single photon counting (TCSPC) (see Supporting Information).

Fig. 3 shows the distributions of the fluorescence lifetime and time-integrated photon counts from single particles for two situations: In Fig. 3A the sample was irradiated with 90% of the maximum laser power (450 μW at the sample), while in Fig. 3B. only 15% of the maximum laser power (75 μW at the sample) was used. In both, Fig. 3A and 3B, as N increases to ~ 200, both photon counts and lifetime decrease. This is consistent with a nonradiative relaxation rate increase due to the concentration quenching effect observed in steady-state spectroscopy (Fig 2B inset and SI). However, as N increases above ～200, bright particles with short lifetimes appear in Fig. 3A but not in Fig. 3B. This is consistent with a significant avoidance of concentration quenching.

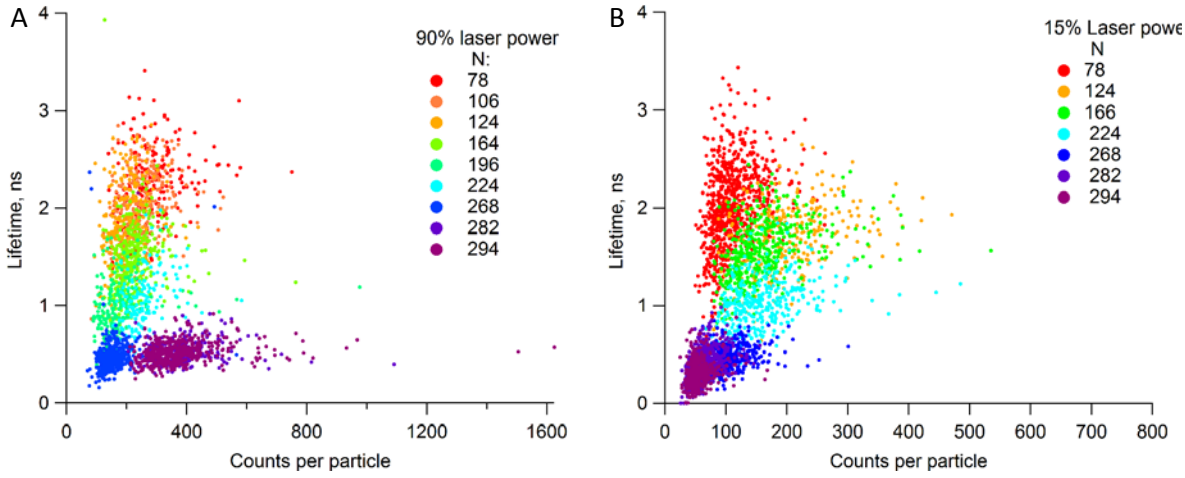

Figure 3. A) Scatter plots of estimated lifetime vs fluorescence photon counts collected from hundreds of labeled BMV particles by single-particle FLIM (each dot represent single virus particle). The different colors represent samples with different average number of chromophores per particle (N). Symbols show the maximum probability point for each distribution. B) Same as (A), except for the excitation power, which is 6x less than in (A).

We consider several possible explanations for the strongly nonlinear behavior in Fig 3A. At the first sight, a possible mechanism could be amplified spontaneous emission (ASE)[27]. In ASE, chromophores absorb light, and start decaying by spontaneous emission. If the emitted light passes through a region containing inverted molecules, it may de-excite these, being amplified in the process. The decay accelerates, shortening the emitted pulse duration. Unlike coherent phenomena, ASE is much less sensitive to phase breaking processes, and therefore we would expect it to occur even in the presence of static and dynamic fluctuations (disorder). To test this idea, we added polyethylene glycol (PEG, MW 6000) to the dye-BMV solution (Fig. 4A). PEG exerts depletion forces on the viral coat protein, and can increase the osmotic pressure on the virus shell[28]. As a result, PEG is known to induce a measurable (~ 10 Å) average radius compression at concentrations above 2.5% [29]. Furthermore, adsorption of PEG is

likely to disrupt the protein/dye interaction and/or change the local environment of the dye[30]. Upon 2.5% PEG addition, the brightening effect observed in Fig. 3A is completely suppressed.

In an additional experiment investigating the role of dye-virus template interaction, we have added a 25 Å linker between the chromophore and the coat protein (see reaction scheme in SI), thus reducing the possibility of chromophore interacting with the virus shell, pushing the chromophore into solution, and making the chromophore more prone to positional fluctuations. Similar to the PEG experiment, this treatment also significantly disrupted the trend in Fig. 3A. Note that, under this approach, some of the dye molecules were still conjugated directly to the surface-exposed lysines, which further added to the heterogeneity of the dye environment (see SI, MALDI data). We conclude that ASE is an unlikely explanation for the observed accelerated decay and the brightening of emission.

Since the density of chromophores in our case is well below that calculated for attaining the stimulated emission threshold in nanolasers[31], the remaining working hypothesis is that the

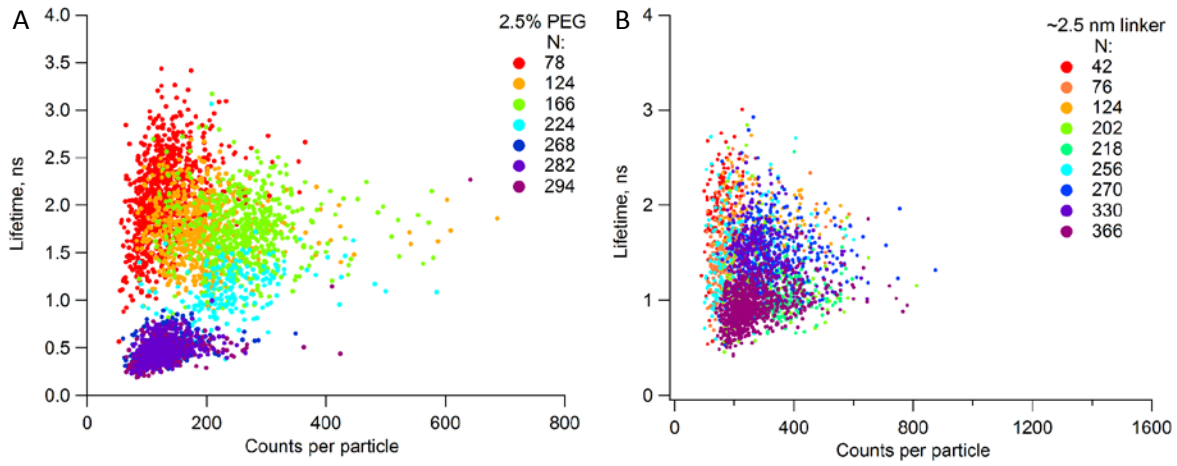

Figure 4. Scatter plots of estimated lifetime vs fluorescence photon counts at same laser power as in Figure 3A but A) in the presence of 2.5% PEG 6000, B) with flexible linker between surface lysines and chromophores.

observed accelerated emission is due to superradiance. Four factors favor this hypothesis: i) immobilization of emitters on a rigid molecular scaffold at identical local environments is expected to lead to a reduction of inhomogeneous broadening by suppressing dynamics along some of the molecular degrees of freedom, ii) the strong dye - virus template interaction may decrease the effectiveness of phase breaking processes, iii) the role played by symmetry suggesting involvement of quantum selection rules, iv) the population inversion requirement.

We note that avoidance of fluorescence quenching is known to occur in photosynthetic organelles, even at low excitation intensity. Thus, while emission from a 0.1 M chlorophyll solution is completely quenched, chlorophylls bound in light harvesting complexes of certain photosynthetic bacteria are strongly fluorescent at room temperature even as the concentration reaches 0.25 - 0.5 M, *i.e.* concentration quenching is effectively suppressed. The reason for this difference is believed to be the result of the spatial organization of chlorophyll molecules in photosynthetic LHCs not being random[32]. The same complexes are believed to exhibit super-radiant behavior at room temperature, in solution, although, it is important to note that in the LHC case, SR is likely of the type observed in molecular aggregates, in stark contrast from the type of molecular organization we are dealing with here.

In conclusion, collective relaxation akin to SR has been achieved in solution, and at room temperature using a biological, virus template approach. A volume much smaller than the wavelength of light, high chromophore densities, and a near perfectly symmetric molecular arrangement, create a set of circumstances in which the photophysical properties of multichromophore particles are significantly different from those of individual chromophores. This discovery may lead to new virus-enabled vectors with qualitatively enhanced optical

emission properties, complemented by possibilities of further chemical or genetic manipulation for targeting in biomedical applications, and potentially other uses that could benefit from bright, deep-subwavelength light sources.

Methods

BMV purification

wtBMV was expressed in Nicotiana benthamiana via Agrobacterium-mediated gene delivery according to previously described protocol[33] . Seven days after infection, N. benthamiana leaves were homogenized in virus buffer [250 mM NaOAc, 10 mM $MgCl_2$ (pH 4.5)] and then centrifuged at 6000 rpm for 25 minutes using an Eppendorf F-35-6-30 rotor. The supernatant was layered on a 10% sucrose cushion in virus buffer and centrifuged at 26,000 rpm for 3 hours using a Beckman SW 32Ti rotor. The pellets were resuspended in 38.5% CsCl (w/v, virus buffer) and were kept overnight in the cold room. Next day, solution was centrifuged at 10,000 rpm for 10 minutes in the BIO-Rad to remove the undissolved pellets. After that, supernatant was centrifuged at 45,000 rpm at 4 ^{o}C in a 100 Ti rotor. The resulting virus band was collected and dialyzed against SAMA [50 mM NaOAc, 8 mM $Mg(OAc)_2$ (pH 4.6)] buffer for 24 hours, with three changes. Virus concentration was measured by Nanodrop.

Fluorescent modification of wtBMV

Surface exposed lysines of wtBMV were labelled by bioconjugation with Oregon Green 488 carboxylic acid, succinimidyl ester. Concentrated stock of wt-BMV was diluted in phosphate buffer (100 mM, pH 8.5) or sodium bicarbonate buffer (100 mM, pH 7.5) to concentration of 10^{13} particles/ml. Dye was freshly prepared in DMSO and mixed with BMV solution at different ratios ranging from 1000 to 20000 dyes/capsid. The reaction was left for 2-3 hours at room temperature, then free dye was removed via dialysis or filter wash with virus storage buffer at

pH 4.5. The wash step was done until there was no presence of free dye in supernatant by UV-Vis.

Bioconjugation of Oregon Green dye through a linker

The concentrated stock of wt-BMV was diluted in phosphate buffer (100 mM, pH 7) to a concentration of 10^{13} particles/ml, followed by reacting with 100x excess of Sulfo-SMCC (sulfosuccinimidyl 4-(N-maleimidomethyl) cyclohexane-1-carboxylate) for 1 hour at room temperature. Excess SMCC was removed from the mixture by passing it through a Sephadex column (PD-10) with multiple washes using SAMA buffer with pH 6. The concentration of the virus in the BMV-SMCC mixture was recorded with Nanodrop, and then a bi-functionalized polyethylene glycol with thiol and amine end was mixed in to react for another hour at room temperature. The concentration of BMV-SMCC linker was determined, and it was subjected to mass spectrometry to analyze the masses. Further, OG488 was added in the same proportions as for BOG samples, followed by removal of excess dye using dialysis.

Transmission Electron Microscopy

Electron-transparent samples were prepared by placing 10 µL of dilute sample onto a carbon-coated copper grid. After 10 min, the excess solution on the grid was removed with filter paper. It was stained with 10 µL of 2% uranyl acetate for 10 minutes and the excess solution was removed by blotting with filter paper. The sample was then left to dry for several minutes. Images were acquired at an accelerating voltage of 80 kV on a JEOL JEM1010 transmission electron microscope and analyzed with the ImageJ Processing Toolkit to estimate the diameters of the particles.

Steady State Absorption and Emission Spectroscopy

Absorbance spectra were recorded with a Varian Cary 100 Bio instrument. The concentration of wtBMV and the labeling efficiency of dyes were obtained from the UV-Visible absorbance spectra. Fluorescence measurements were done on a QuantaMaster™ fluorescence spectrometer (Horiba) with the following parameters: excitation wavelength: 488 nm; emission wavelength: 515 nm. The excitation and steady state emission spectra of 100 nM solutions were an average from at least three independent measurements. wt-BMV and OG488 were used as reference standards whose optical characteristics were compared against labeled-BMV.

Fluorescence Lifetime Imaging Microscopy (FLIM)

The lifetime measurements were carried out with **a** Leica TCS SP8 SMD in FLIM configuration. The sample was excited at a wavelength of 488 nm from a supercontinuum laser emitting pulses of 120 ps at 40 MHz. The time-average maximum power was 500 µW at the sample. The collection spectral window was 500 nm to 550 nm. Data analysis was done with SymPhoTime 64 (PicoQuant) software, ImageJ Processing Toolkit, and IgorPro.

Matrix Assisted Laser Desorption/Ionization-Time of Flight Spectrometry

Fluorescent dye labeled BMV samples were buffer-exchanged to water. The diluted samples were mixed with α-cyano-4-hydroxycinnamic acid (CCA) matrix in 1:5 ratio (varies depending upon the concentration of the sample. Myoglobin and CytochromeC protein mixture was used as the calibrant, which was introduced in 1:1:5 ratio with respect to the CCA matrix. Matrix Assisted Laser Desorption/Ionization- Time of Flight (MALDI-TOF) Mass Spectrometry was done

on Bruker Autoflex III in the linear mode. A 355 nm frequency tripled beam Nd-YAG laser was incident on the 384-well steel plate of 1µL spot size.

Cryo-electron microscopy

Cryo-EM frozen hydrated specimen was prepared as follows: 4 µL sample of Oregon Green labelled BMV capsid was loaded onto a glow-discharged Quantifoil R2/2 300 meshed copper grid that has an addition ultrathin layer of carbon film. The grid was quickly frozen by using a FEI Vitrobot^{TM} Mark III. The humidity in the chamber was set to 100% and the blotting time is 4 sec. The frozen hydrated specimen was then transferred to a Gatan 626 cryo-holder and kept under liquid nitrogen temperature (approximately -172°C) for the subsequently data collection. The grid was imaged using a 300-kV JEOL JEM-3200FS equipped with in-column energy filter and a DE-64 direct electron detection camera. The energy slit width was set to 20 eV and a nominal magnification of x60000 (equivalent to 0.854 Å per pixel) was used to collect the 141 25-frame movie stacks. The movie stacks were aligned, dose-weighted, and summed using MotionCor2 [34]. The first 2 and the last 10 frames were discarded, leaving the total dose to be less than 30 $e^-/Å^2$. The defocus value for each micrograph was estimated using CTFFIND4 [35]. A total of 31378 particles were semi-manually picked using e2boxer.py [36]. Reference-free 2D classification was performed on the whole particle set using Relion 2.1 [37] and the particles within class averages that are shown to be either clear noise or significant overlap were discarded at this point. The class averages that show clear capsomer density were then used to build the initial low-resolution model using e2initialmodel.py. This initial model was further refined using Relion 3D auto-refine with a total of 12522 particles and a post-processing procedure to a final resolution of 7 Å. The 3D model of Oregon Green labeled BMV was

visualized and analyzed using UCSF Chimera [38]. The atomic coordinates of native BMV (PDB code 1SJ9) solved by X-ray crystallography was fitted into the cryo-EM density to analyze the potential binding positions for Oregon Green.

References

1 Stepanenko, O. V. *et al.* Modern fluorescent proteins: from chromophore formation to novel intracellular applications. *BioTechniques* **51**, 313-314, 316, 318 passim, doi:10.2144/000113765 (2011).

2 Tsien, R. Y. Nobel Lecture: Constructing and Exploiting the Fluorescent Protein Paintbox. (2008).

3 Hong, G., Antaris, A. L. & Dai, H. Near-infrared fluorophores for biomedical imaging. *Nature Biomedical Engineering* **1**, 0010, doi:10.1038/s41551-016-0010 (2017).

4 Khitrova, G. & Gibbs, H. M. Collective radiance. *Nature Physics* **3**, 84-85, doi:10.1038/nphys532 (2007).

5 Dicke, R. H. Coherence in Spontaneous Radiation Processes. *Physical Review* **93**, 99-110 (1954).

6 Ball, P. Physics of life: The dawn of quantum biology. *Nature* **474**, 272-274, doi:10.1038/474272a (2011).

7 Scholes, G. D., Fleming, G. R., Olaya-Castro, A. & van Grondelle, R. Lessons from nature about solar light harvesting. *Nature Chemistry* **3**, 763, doi:10.1038/nchem.1145 (2011).

8 Monshouwer, R., Abrahamsson, M., van Mourik, F. & van Grondelle, R. Superradiance and Exciton Delocalization in Bacterial Photosynthetic Light-Harvesting Systems. *The Journal of Physical Chemistry B* **101**, 7241-7248, doi:10.1021/jp963377t (1997).

9 Senders, J. T. *et al.* Agents for fluorescence-guided glioma surgery: a systematic review of preclinical and clinical results. *Acta Neurochirurgica* **159**, 151-167, doi:10.1007/s00701-016-3028-5 (2017).

10 Nguyen, Q. T. & Tsien, R. Y. Fluorescence-guided surgery with live molecular navigation — a new cutting edge. *Nature reviews. Cancer* **13**, 653-662, doi:10.1038/nrc3566 (2013).

11 Wu, X. *et al.* Dye-Sensitized Core/Active Shell Upconversion Nanoparticles for Optogenetics and Bioimaging Applications. *ACS Nano* **10**, 1060-1066, doi:10.1021/acsnano.5b06383 (2016).

12 Koenderink, A. F., Alù, A. & Polman, A. Nanophotonics: Shrinking light-based technology. *Science* **348**, 516 (2015).

13 Purcell, E. M. in *Confined Electrons and Photons NATO ASI Series (Series B: Physics)* (eds E. Burstein & C. Weisbuch) vol 340, pp 839-839 (Springer US, 1995).

14 Purcell, E. M. in *Proceedings of the American Physical Society, 1946.*

15 Benedict, M. G. *Super-radiance: Multiatomic Coherent Emission*. (Taylor & Francis Group, LLC, 1996).

16 Skribanowitz, N., Herman, I. P., MacGillivray, J. C. & Feld, M. S. Observation of Dicke Superradiance in Optically Pumped HF Gas. *Physical Review Letters* **30**, 309-312 (1973).

17 Gross, M., Fabre, C., Pillet, P. & Haroche, S. Observation of Near-Infrared Dicke Superradiance on Cascading Transitions in Atomic Sodium. *Physical Review Letters* **36**, 1035-1038 (1976).

18 Dicke, R. H. Coherence in Spontaneous Radiation Processes. *Phys. Rev.* **93**, 99-110, doi:10.1103/PhysRev.93.99 (1954).

19 Florian, R., Schwan, L. O. & Schmid, D. Superradiance and high-gain mirrorless laser activity of O−2-centers in KCl. *Solid State Communications* **42**, 55-57, doi:10.1016/0038-1098(82)91028-6 (1982).

20 Scheibner, M. *et al.* Superradiance of quantum dots. *Nature Physics* **3**, 106, doi:10.1038/nphys494 (2007).

21 Frolov, S. V., Gellermann, W., Ozaki, M., Yoshino, K. & Vardeny, Z. V. Cooperative Emission in π-Conjugated Polymer Thin Films. *Physical Review Letters* **78**, 729-732 (1997).

22 Bradac, C. *et al.* Room-temperature spontaneous superradiance from single diamond nanocrystals. *Nature Communications* **8**, 1205-1205, doi:10.1038/s41467-017-01397-4 (2017).

23 Lucas, R., Larson, S. & McPherson, A. The crystallographic structure of brome mosaic virus. *Journal of Molecular Biology* **317**, 95-108, doi:10.1006/jmbi.2001.5389 (2002).
24 Running, W. E., Ni, P., Kao, C. C. & Reilly, J. P. Chemical reactivity of brome mosaic virus capsid protein. *Journal of molecular biology* **423**, 79-95, doi:10.1016/j.jmb.2012.06.031 (2012).
25 Spano, F. C. The Spectral Signatures of Frenkel Polarons in H- and J-Aggregates. *Accounts of Chemical Research* **43**, 429-439, doi:10.1021/ar900233v (2010).
26 Soto, C. M. *et al.* Fluorescent Signal Amplification of Carbocyanine Dyes Using Engineered Viral Nanoparticles. *Journal of the American Chemical Society* **128**, 5184-5189, doi:10.1021/ja058574x (2006).
27 Schuurmans, M. F. H. & Polder, D. Superfluorescence and amplified spontaneous emission: A unified theory. *Physics Letters A* **72**, 306-308, doi:10.1016/0375-9601(79)90477-8 (1979).
28 Gelbart, W. M. & Knobler, C. M. VIROLOGY: Pressurized Viruses. *Science (New York, NY)* **323**, 1682-1683 (2009).
29 Zeng, C. *Structure and mechanochemistry of icosahedral viruses and virus shells studied by atomic force microscopy* Ph.D. thesis, Indiana University, (2017).
30 Knowles, D. B. *et al.* Chemical Interactions of Polyethylene Glycols (PEG) and Glycerol with Protein Functional Groups: Applications to PEG, Glycerol Effects on Protein Processes. *Biochemistry* **54**, 3528-3542, doi:10.1021/acs.biochem.5b00246 (2015).
31 Shahbazyan, T. V. Mode Volume, Energy Transfer, and Spaser Threshold in Plasmonic Systems with Gain. *ACS Photonics* **4**, 1003-1008, doi:10.1021/acsphotonics.7b00088 (2017).
32 Beddard, G. S. & Porter, G. Concentration quenching in chlorophyll. *Nature* **260**, 366, doi:10.1038/260366a0 (1976).
33 Gopinath, K. & Kao, C. C. Replication-Independent Long-Distance Trafficking by Viral RNAs in Nicotiana benthamiana. *The Plant Cell* **19**, 1179-1191, doi:10.1105/tpc.107.050088 (2007).
34 Zheng, S. Q. *et al.* MotionCor2: anisotropic correction of beam-induced motion for improved cryo-electron microscopy. *Nat Methods* **14**, 331-332, doi:10.1038/nmeth.4193 (2017).
35 Rohou, A. & Grigorieff, N. CTFFIND4: Fast and accurate defocus estimation from electron micrographs. *J Struct Biol* **192**, 216-221, doi:10.1016/j.jsb.2015.08.008 (2015).
36 Tang, G. *et al.* EMAN2: an extensible image processing suite for electron microscopy. *J Struct Biol* **157**, 38-46, doi:10.1016/j.jsb.2006.05.009 (2007).
37 Scheres, S. H. RELION: implementation of a Bayesian approach to cryo-EM structure determination. *J Struct Biol* **180**, 519-530, doi:10.1016/j.jsb.2012.09.006 (2012).
38 Pettersen, E. F. *et al.* UCSF Chimera--a visualization system for exploratory research and analysis. *J Comput Chem* **25**, 1605-1612, doi:10.1002/jcc.20084 (2004).

Acknowledgements: The authors gratefully acknowledge support for this work from the U.S. Army Research Office through award #W911NF1310490, and from the National Science Foundation through award #1740432. The authors also thank Dr. T. Shahbazyan for insightful discussions and comments on this work.

Author contributions: I.T. and A.A.S. synthesized the samples and performed the experiments, I.T. processed the data and wrote a first draft of the manuscript, J.C.-Y.W. performed the cryo-em

342 experiments and structural analysis, WLS contributed to the drafting and critical revision of the
343 manuscript, B.D. conceived and designed the research, and contributed to data analysis and manuscript
344 preparation.

345 **Supplementary information** is available for this paper

Supporting information for

Collective emission from arrays of virus-supported chromophores

Irina B. Tsvetkova[a], Arathi Anil Sushma[a], Joseph C.-Y. Wang[b], William L. Schaich[c], and Bogdan G. Dragnea[a]*

[a]Chemistry Department, Indiana University Bloomington, IN, 47405, USA

[b]Department of Molecular and Cellular Biochemistry, Indiana University Bloomington, IN, 47405, USA

[c]Physics Department, Indiana University Bloomington, IN, 47405, USA

*Correspondence and requests for materials should be addressed to B.D. (email: dragnea@indiana.edu)

Virus modification and characterization

Virions of the Brome mosaic virus (BMV), with T = 3 icosahedral symmetry provided the symmetric template for bio-conjugation[7]. The 28 nm-diameter BMV capsid is composed of 180 identical copies of a single coat protein. BMV can be disassembled into protein dimers and RNA genome and reassembled[8]. Conditions for obtaining empty virus-like particles [9] or hybrid nanoparticles containing synthetic cores[10-12] have been extensively studied.

The chemical surface modification of BMV capsid has been studied [13]. wtBMV has 12 lysines per coat protein among which residues K64, K83, K105, K111, and K165 (Fig. 1A, S1) are surface-exposed and have been shown to efficiently undergo chemical modification by thioimidate reagents [14]. These reactive lysines provide, in principle, for 900 possible labeling sites on the virus surface, for further modification. We analyzed the likelihood of dye locations and nearest-neighbor distances on the surface of BMV by measuring distances between lysines residues in the full virus molecular model using the Chimera software. The average nearest distance between reactive surface exposed lysines is about 2 nm (Fig. SI1).

Lysines are commonly addressed through reaction with active esters (e.g, succinimidyl, sulfosuccinimidyl, or tetrafluorophenyl esters) [15] (Fig. 1B). Changing the molar ratio of chromophores to the virus in the reaction media varied the average number of chromophores. The labeling reaction was done in two buffer conditions to obtain better control over N. Fig. SI2 shows the dependence of <N> on the dye input concentration at the reaction onset.

The efficiency of labeling in BMV-chromophore conjugates was determined by UV-Visible absorption spectroscopy and supported by Matrix Assisted Laser Desorption/Ionization-

A

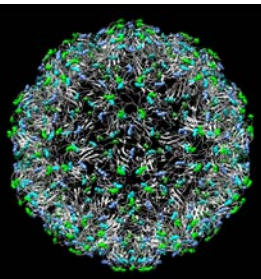

K64 - pentamer/hexamer (upper)
K83 - trimer (lower)
K105 - pentamer/hexamer (lower)
K111 - trimer (upper)
K165 – “dimer”

All distances are in Å

B

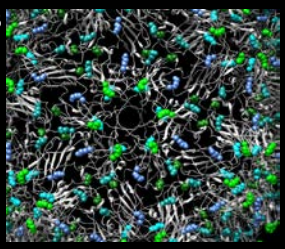

hexamer	64	83	105	111	165
64	18-20	34-39	11-18	27-28	23-25
83	34-39	13-18	27-29	11-15	21-24
105	11-18	27-29	18-19	24-25	20-21
111	27-28	11-15	24-25	14-19	22-24
165	23-25	21-24	20-21	22-24	16

C

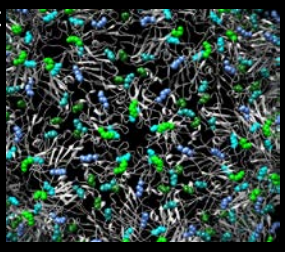

pentamer	64	83	105	111	165
64	17-28	32-38	9-17	27-39	24-26
83	32-38	13-18	28-35	11-15	21-24
105	9-17	28-35	13-21	27-34	24-27
111	27-39	11-15	27-34	14-19	22-24
165	24 -26	21-24	24-27	22-24	16

Figure SI1. Analysis of distances between possible labelling sites. A) Full virus model and color description, B) hexamer view and table with distances for hexameric subunit, C) same as B but for pentameric subunit. Note: From structure analysis K165, K64, K11 are likely to be labelled and K83 and K105 are less likely.

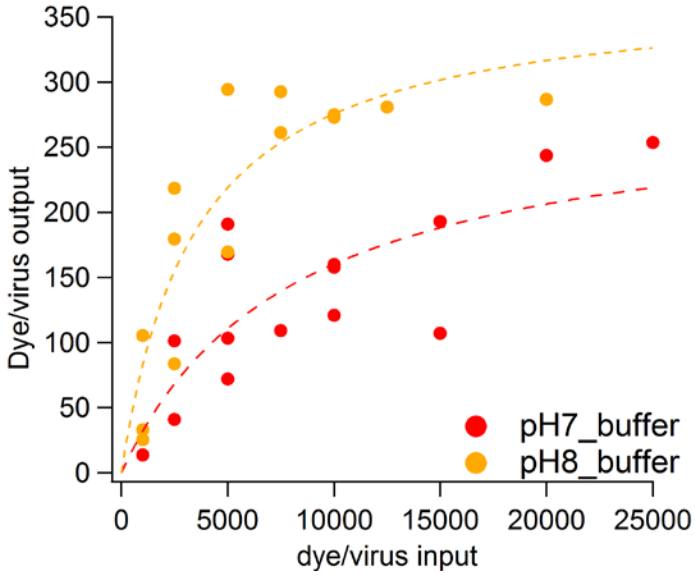

Figure SI2. Bioconjugation reaction output vs dye input in reaction mixture for two buffer conditions (dashed lines are binding isotherm fitting).

Time of Flight Spectrometry (MALDI-TOF). The average number of chromophores per particle was calculated from extinction data using the Beer-Lambert law and the molar extinction coefficient (ε = 70,000$cm^{-1}M^{-1}$) for Oregon green at 496 nm in buffer at pH 8. BMV is most stable in buffers with pH 4-5. Therefore concentration measurements were done in these conditions. As a consequence of the pH change, the extinction coefficient had to be adjusted. In order to do account for the change in the extinction coefficient, the free dye absorbance spectrum was measured for a pH range from 4 to 8 at varied concentrations from 0.05 uM to 0.5 uM. Thus we obtained an ε at pH 4.6 of 33641$cm^{-1}M^{-1}$.

MALDI-TOF (Fig. SI3) was used to provide molecular weight information of labeled proteins. For BMV labeled through lysine modification, there are two peaks present below 200 dyes/virus, which correspond to unlabeled protein and proteins with one dye. For samples with a dye/virus ratio of above 200, a third peak appeared which corresponds to two dyes per coat protein. Also, the height of unlabeled protein peak decreased significantly. By fitting the peaks we can estimate the degree of labeling from MALDI experiments. The table in Figure SI3 provides the comparison between the labeling load calculated from UV-Vis spectra and from MALDI-TOF spectra. Although there is a difference in absolute numbers between two methods, the trend is the same. It is likely that MALDI-TOF underestimates the degree of labeling due to the particle stability against laser-induced fragmentation being dependent on labeling.

Particle morphology was imaged by negative stained TEM and Cryo-EM images and dye-conjugated BMV is indistinguishable from wtBMV (Fig. SI4). The inset in Fig SI4A shows the rotationally averaged particle image with two structural layers: the outer capsid layer and the inner RNA layer. No observable disruption on the labeled capsid surface can be detected

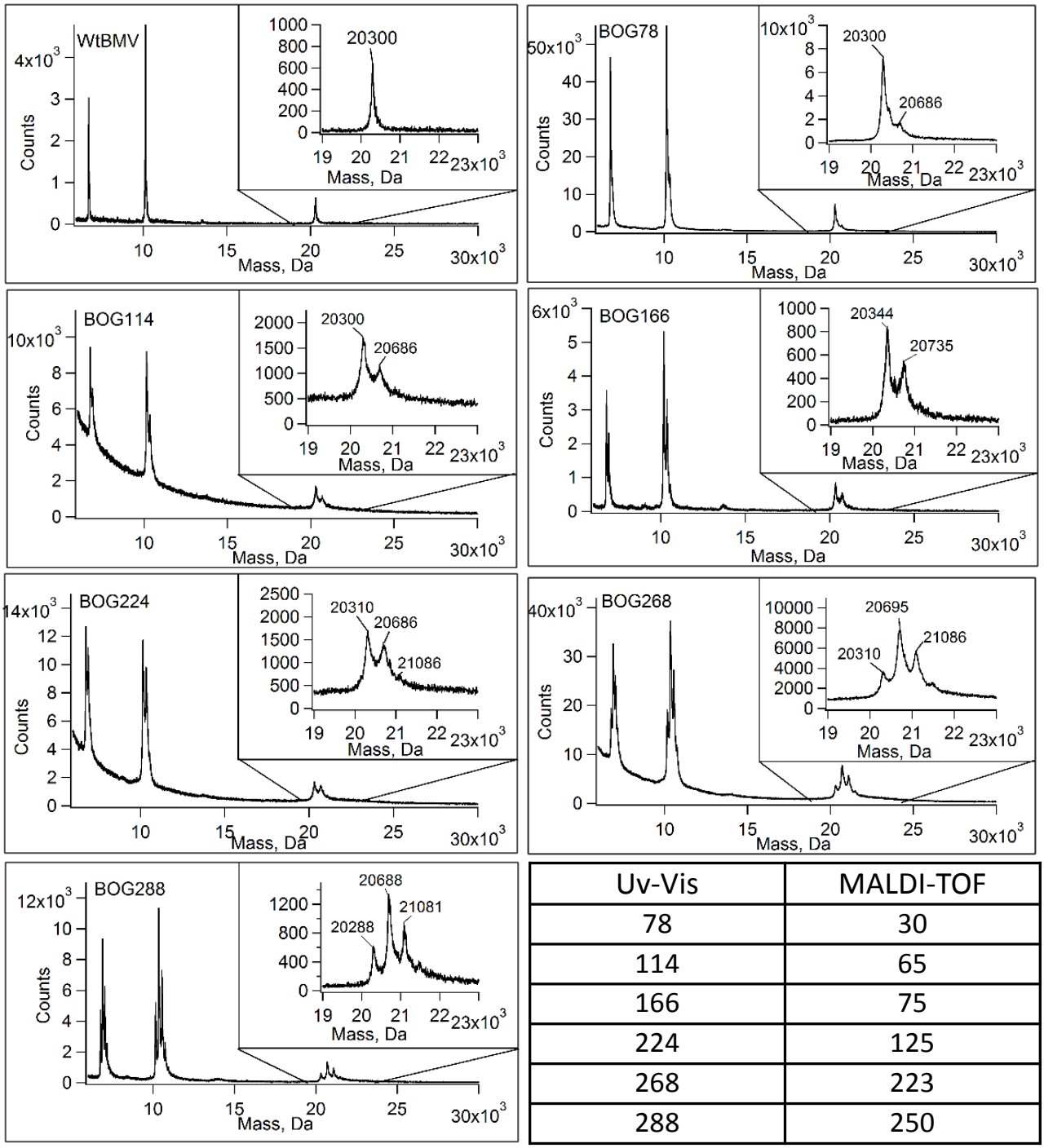

Uv-Vis	MALDI-TOF
78	30
114	65
166	75
224	125
268	223
288	250

Figure SI3. MALDI-TOF spectra for wtBMV and bioconjugated samples with different N and table with comparison of dye loading calculated from UV-Vis and MALDI spectra.

62

(Fig SI4B). A total of 12522 particles from 141 micrographs were used to compute the final 3D reconstruction to 7Å resolution (estimated by Fourier shell correlation at 0.143). At the 3D level, the labeled BMV capsid also exhibits an overall architecture of T=3 surface lattice that is comparable to the native virus (Fig SI4C). There are 12 pentameric capsomer protrusions located at the fivefold axes and 20 hexameric capsomer protrusions located at threefold axes. Docking of the X-ray crystallographic structure (PDB code 1JS9) into the cryo-EM density map

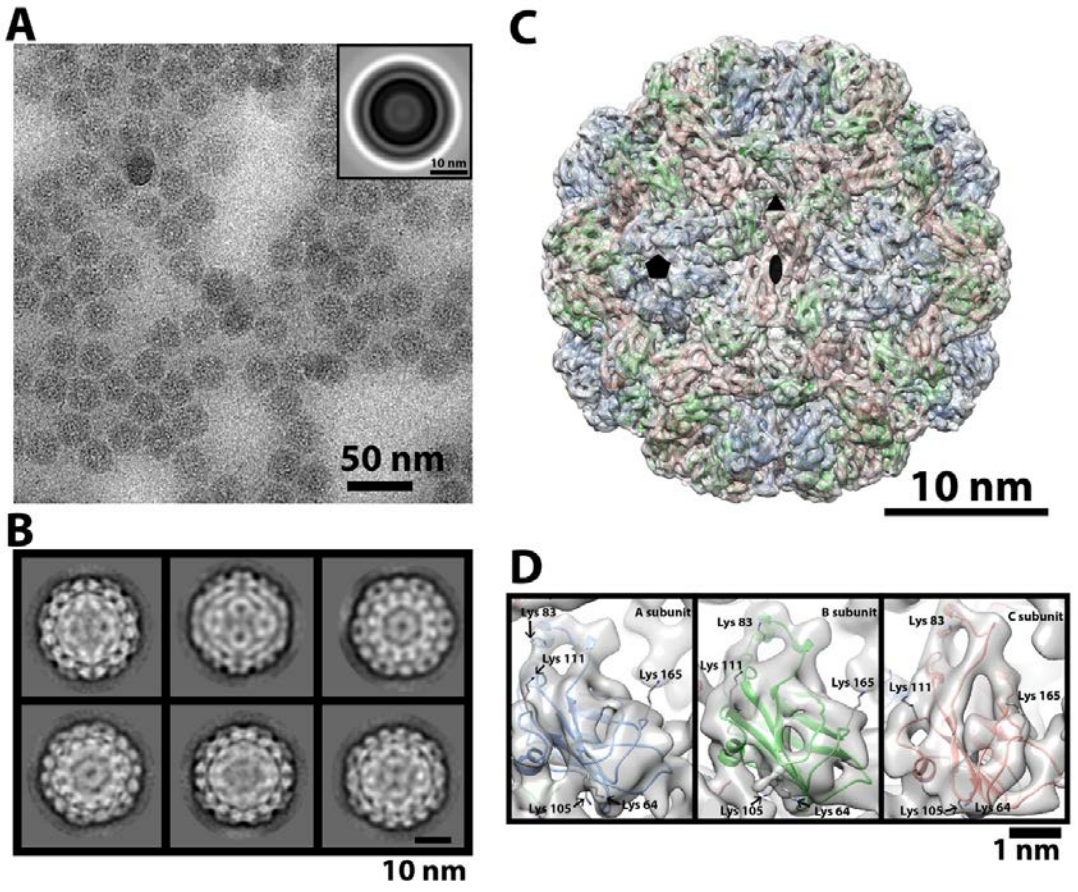

Figure SI4. Cryo-EM analysis of Oregon Green labeled BMV. (A) A representative cryo-EM micrograph of BMV particles vitrified in a thin layer of ice. Inset shows the rotationally aligned averaged image. (B) Selected typical class averages calculated from reference-free 2D classification. (C) The cryo-EM structure of Oregon Green labeled BMV (transparent grey) fitted with the atomic structure of BMV (PDB code 1JS8). (D) Close-up views of each subunits show Lys 64 has become buried within the electron density map.

reveals excellent agreement (Fig SI4C). Out of five possible locations on the BMV capsid protein that may interact with Oregon Green: Lys 64, Lys 83, Lys 105, Lys 111, and Lys 165. Lys 64 was found to be mostly buried inside the cryo-EM density (FigSI4D). Other Lys positions are either partially exposed or fully exposed.

Since at the current resolution in the cryo-EM reconstruction no extra density could be attributed to Oregon Green molecule, we surmise the dye must be very close to the BMV surface. This is supported by the dye-conjugated BMV particles being more stable to physical and chemical manipulations with respect to wtBMV, which suggests that the chromophore interacts strongly with the capsid, stabilizing it. Specifically, when dialyzed in disassembly buffer

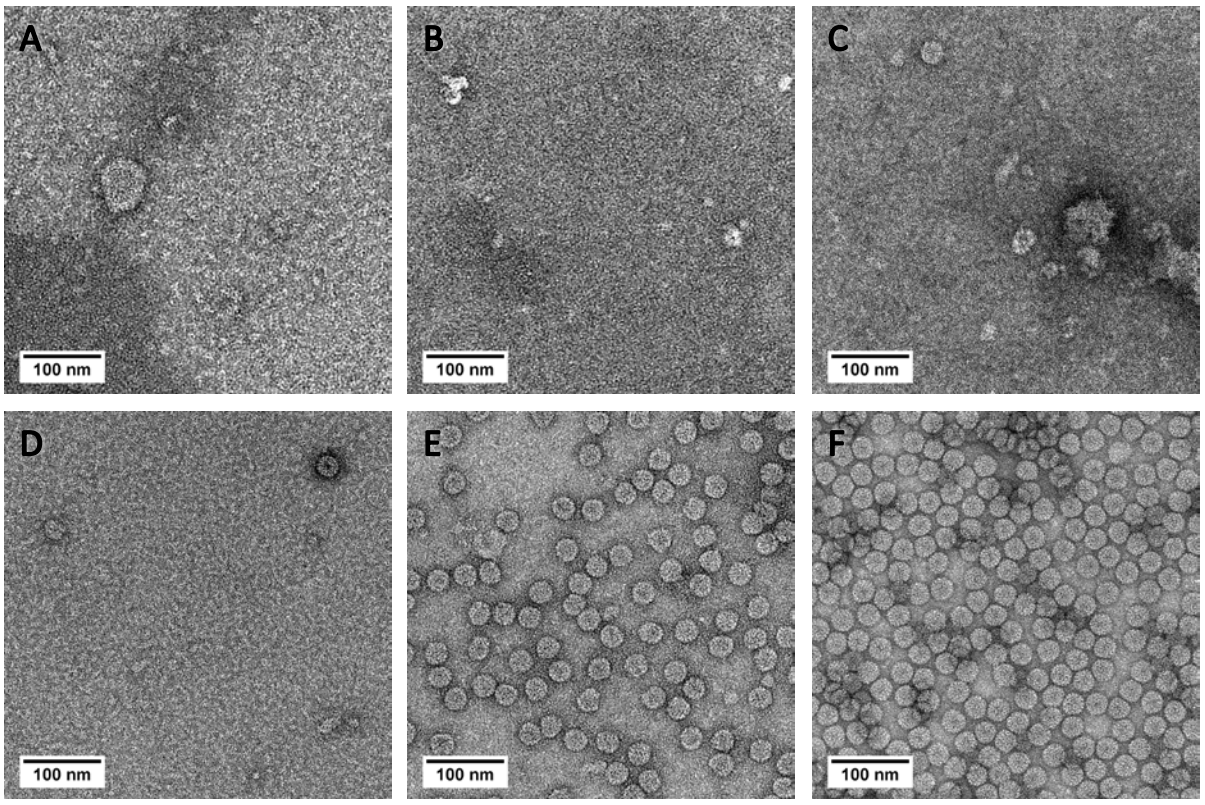

Figure SI5. Stability test. TEM images of samples after overnight dialysis in disassembly buffer: A) wtBMV, B) BOG74 , C) BOG 196, D) BOG 224, E) BOG 268 and F) BOG 288 after drying-reconstitution cycle.

conditions for 24 hours, wtBMV is completely disassembled (Fig. SI5A) but dye-conjugated BMV with dye ratio above 200 has the same morphology as in virus-storage buffer (Fig. SI5D-E). Additionally, the <N>=288 sample was completely dried under vacuum overnight and reconstituted with SAMA buffer. Again, the <N> = 288 virus particles retained their native morphology and optical properties (by FLIM).

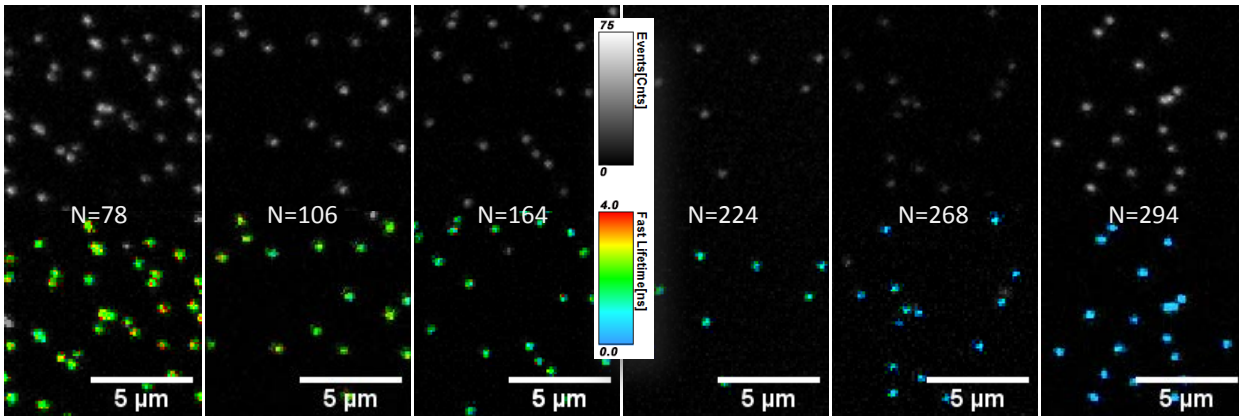

Figure SI6. FLIM images of single particles: photon counts (top row) decreases until N>200 and mean of photon arrival times (bottom row) decreasing from 3.5 ns to 0.5 ns.

Fluorescence life-time imaging considerations

FLIM images are presented in Figure SI6. Non-monotonic changes of photon counts (grey scale) and lifetime (color scale) as function of the average number of dyes per virus particle are visible. The scatter plots presented in the main text were obtained by integrating the photon counts from single virus areas and measuring the mean of photon arrival times for at least 200 single virus particles, and from at least 5 images obtained from different regions in the sample.

We used the mean photon arrival time per pixel as a measure of the single particle lifetime instead of a histogram fit due to the noise in the individual histograms of arrival times at low counts per pixel. In support for this approach giving a fair representation of the lifetime, we integrated the arrival times over all pixels associated with virus particles and used the ensemble histogram for exponential fitting to find the overall sample lifetime. The value thus obtained matched well the averaged mean photon arrival time per pixel.

It is important to note here that the fluorescence life-time microscopy setup is based on the time correlated single photon counting (TCSPC) scheme. While this scheme clearly indicates that the emitted number of photons depends non-linearly on <N>, for quantitative studies TCSPC has the drawback that it relies on the assumption of uncorrelated photon emission statistics, more specifically, on the assumption of one or less photons per pulse. Thus, after the excitation pulse, detection of arrival of the first emitted photon triggers the readout and one event is recorded in the histogram at the arrival time. The TCSPC card is not able to count for a period known as “dead-time” after this event, which in our case is 90 ns. For correlated photons, counts and lifetimes may appear skewed when the TCSPC scheme is used. Work is underway to implement a second-order photon correlation setup, which will be able to provide the true photon correlation statistics.

It is worth noting that at the maximum laser power employed in our setup, we expect photon emission at each pulse. With this assumption and taking into account losses in FLIM set-up (reflections, detector quantum yield, and electronics dead time) we calculated the maximum measurement limit to be 60 photon counts/pixel. By integration over 9 pixels/particle, to include all photons from a single virus, the maximum counts for particle emitted at every pulse,

is in the range of 300-350 counts/particle (because of bell-shaped point-spread function). This is also the maximum we have obtained for samples with N>200. Therefore, the maximum counts obtained for samples with N>200, supports efficient excitation and subsequent emission at every pulse. This is only possible if we assume collective relaxation is more effective than non-radiative quenching.

Additional supporting images for control sample characterization:

The flexible linker was added between chromophore and virus surface by first reacting the lysines with hetero-bifunctional SMCC (succinimidyl 4-(N-maleimidomethyl)cyclohexane-1-carboxylate, ~8 Å long) and then, adding thiol-TEG-NH_2 (~17 Å long), followed by conjugation of OG-488 dye (Fig. SI8A). In this case, it should be noted that some of the dyes were attached to the surface exposed lysines, adding to the heterogeneity of the system and further disrupting symmetry (Fig. SI8B).

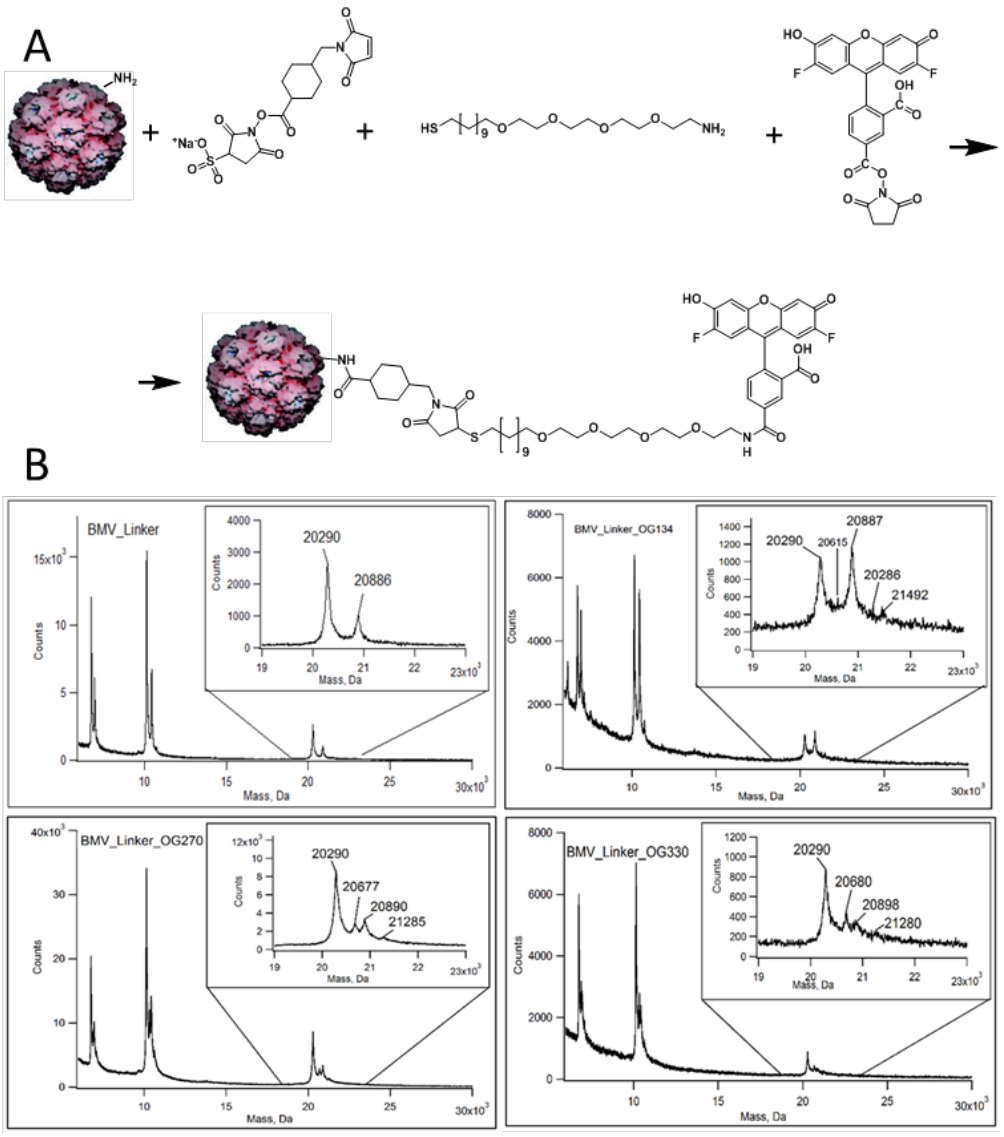

Figure SI8. A) Scheme of bioconjugation through a linker, MALDI-TOF spectra for BMV with flexible linker and samples with dye attached through linker for different N.

127

128

References

1 Miller, R. A., Presley, A. D. & Francis, M. B. Self-Assembling Light-Harvesting Systems from Synthetically Modified Tobacco Mosaic Virus Coat Proteins. *Journal of the American Chemical Society* **129**, 3104-3109, doi:10.1021/ja063887t (2007).

2 Park, H. *et al.* Enhanced energy transport in genetically engineered excitonic networks. *Nature Materials* **15**, 211, doi:10.1038/nmat4448 (2015).

3 Noriega, R. *et al.* Manipulating Excited-State Dynamics of Individual Light-Harvesting Chromophores through Restricted Motions in a Hydrated Nanoscale Protein Cavity. *The Journal of Physical Chemistry B* **119**, 6963-6973, doi:10.1021/acs.jpcb.5b03784 (2015).

4 Soto, C. M. *et al.* Fluorescent Signal Amplification of Carbocyanine Dyes Using Engineered Viral Nanoparticles. *Journal of the American Chemical Society* **128**, 5184-5189, doi:10.1021/ja058574x (2006).

5 Wen, A. M. *et al.* Interface of Physics and Biology: Engineering Virus-Based Nanoparticles for Biophotonics. *Bioconjugate Chemistry* **26**, 51-62, doi:10.1021/bc500524f (2015).

6 Wen, A. M. & Steinmetz, N. F. Design of virus-based nanomaterials for medicine, biotechnology, and energy. *Chemical Society Reviews* **45**, 4074-4126, doi:10.1039/C5CS00287G (2016).

7 Lucas, R., Larson, S. & McPherson, A. The crystallographic structure of brome mosaic virus. *J Mol Biol* **317**, 95-108, doi:10.1006/jmbi.2001.5389 (2002).

8 Cuillel, M., Berthetcolominas, C., Timmins, P. A. & Zulauf, M. Reassembly of Brome Mosaic-virus from dissociated virus - a neutron-scattering study. *Eur. Biophys. J.* **15**, 169-176 (1987).

9 Pfeiffer, F., Herzog, M. & Hirth, L. RNA viruses - Stabilization of brome mozaic virus. *Philosophical Transactions of the Royal Society of London. B, Biological Sciences* **276**, 99 (1976).

10 Sun, J. *et al.* Core-controlled polymorphism in virus-like particles. *PNAS* **104**, 1354-1359, doi:10.1073/pnas.0610542104 (2007).

11 Huang, X. *et al.* Self-assembled virus-like particles with magnetic cores. *Nano Lett.* **7**, 2407-2416, doi:10.1021/nl071083l (2007).

12 Dixit, S. K. *et al.* Quantum dot encapsulation in viral capsids. *Nano Lett.* **6**, 1993-1999, doi:10.1021/nl061165u (2006).

13 Yildiz, I. *et al.* Engineering of Brome mosaic virus for biomedical applications. *Rsc Adv* **2**, 3670-3677, doi:10.1039/c2ra01376b (2012).

14 Running, W. E., Ni, P., Kao, C. C. & Reilly, J. P. Chemical reactivity of brome mosaic virus capsid protein. *Journal of molecular biology* **423**, 79-95, doi:10.1016/j.jmb.2012.06.031 (2012).

15 *The Molecular Probes Handbook : a guide to fluorescent probes and labeling technologies.* 11th Edition edn, 1060 (Life Technologies, 2010).

16 Patting, M. *et al.* Fluorescence decay data analysis correcting for detector pulse pile-up at very high count rates. (2017).